Chapter

The Phenomenon of Friction Resistance Due to Streamwise Heterogeneous Roughness with Modified Wall-Function RANSE

I. Ketut Aria Pria Utama, I. Ketut Suastika and Muhammad Luqman Hakim

Abstract

Surface roughness can reduce the performance of a system of fluid mechanics due to an increase in frictional resistance. The ship hull, which is overgrown by biofouling, experiences a drag penalty which causes energy wastage and increased emission levels. The phenomenon of fluid flow that passes over a rough surface still has many questions, one of which is the phenomenon of frictional resistance on heterogeneous roughness in the streamwise direction. In the ship hull, biofouling generally grows heterogeneous along the hull with many factors. RANSE-based Computational Fluid Dynamics was used to investigate the friction resistance for heterogeneous roughness phenomenon. The modified wall-function method represented equivalent sand grain roughness (k_s) and a roughness function were applied together with k-epsilon turbulence model to simulate rough wall turbulent boundary layer flow. As the heterogeneous roughness, three different k_s values were denoted as P (k_s = 81.25 μm), Q (k_s = 325.00 μm) and R (k_s = 568.75 μm), and they are arranged by all possible combinations. The combined roughness, whether homogeneous (PPP, QQQ, or RRR) and inhomogeneous (PQR, PRQ, QPR, etc.), results in unique skin friction values. The step-change in the height of the heterogeneous roughness produced a sudden change in the local skin friction coefficient in the form of overshoot or undershoot, followed by a relaxation where the inhomogeneous local skin friction is slowly returning to the homogeneous local one, which was explained in more detail by plotting the distribution of the mean velocity profile near the step-up or step-down. The order of roughness arrangement in a streamwise heterogenous roughness pattern plays a key role in generating overall skin friction with values increasing in the following order: PQR < PRQ < QPR < QRP < RPQ < RQP. Those inhomogeneous cases with three different values of k_s can be represented by a single value (being like homogeneous) by the calculations provided in this paper.

Keywords: Heterogeneous roughness, Inhomogeneous roughness, RANSE simulations, Skin friction, modified wall-function

1. Introduction

The issue of using energy more efficiently on ships seems urgent, and how to do this is greatly helped by the existence of CFD. In the last three decades, CFD as a numerical method, which is very sophisticated that can help humans to solve various problems in the fields of science and technology [1–6], but at a competitive cost, has played a very important role in advancing transportation technology [7], especially in naval architecture [8]. With this highly sophisticated method, the need for increased energy efficiency on ships is greatly helped. In 2012, the International Maritime Organization (IMO) noted that the total emissions from the shipping sector worldwide were 2.2% compared to all human-made CO_2 emissions [9]. This number was predicted to increase 2–3 times in 2050 if there are no prevention efforts [10]. There are many ways to save on the use of energy on board [11, 12], such as improving hull and propeller design for more hydrodynamic performance. With the help of CFD, efforts to improve energy efficiency can be made more accessible.

Caring about the cleanliness of the hull due to biofouling is one of the efforts to maintain the hydrodynamic performance to prevent energy waste. Roughness can increase friction resistance, and then power requirements increase, resulting in losses, which have a significant impact on large vessels such as the VLCC (Very Large Crude Carrier) [13] or ships with low Fr (Froude number) [14]. A roughness, namely tubeworm fouling, can increase the friction resistance of ships by 23–34% [15], while a heavily fouled ship hull can increase the friction resistance by up to 80% [16]. Due to the growth of biofouling on ship hull, fuel consumption can increase over the operational time and can increase significantly just in a year [17]. The total economic losses from biofouling, including fuel additions, cleaning, and repainting, can reach $ 15 million a year [18].

The phenomenon of the effect of roughness on fluid flow was first investigated by Nikuradse [19]. The mean velocity profile of the structure turbulence boundary layer of the smooth case (see Eq. (1)) is exposed to a downward shift in the log law region by a roughness to become a new velocity profile (see Eq. (2)) [20]. Thus, the concept of the roughness function (ΔU^+) as the downward shift and the roughness Reynold number ($k_s{}^+$) were used (see Eqs. 3 and 4). Where: U^+ is the non-dimensional mean velocity profile equal to U/U_τ; U is the mean velocity at y (the normal from the wall); U_τ is the friction velocity defined as $\sqrt{\tau_w/\rho}$; τ_w is the shear stress magnitude and ρ is the density of the fluid; y^+ is the non-dimensional normal distance from the wall defined as yU_τ/ν; ν is the kinematic viscosity; κ is the von Karman constant and B is the smooth wall log-law intercept; k_s is equivalent sand roughness height. From the new velocity profile, there is an indication of an increased momentum deficit compared to the smooth case.

$$U^+{}_{smooth} = \frac{1}{\kappa} \ln y^+ + B \tag{1}$$

$$U^+{}_{rough} = \frac{1}{\kappa} \ln y^+ + B - \Delta U^+ \tag{2}$$

$$\Delta U^+ = f\left(k_s{}^+\right) \tag{3}$$

$$k_s{}^+ = \frac{k_s U_\tau}{\nu} \tag{4}$$

The flow over surface roughness phenomenon can be simulated using CFD, which is generally solved by two different methods: modified wall function and

geometrically resolved. The modified wall function is a method in which the geometry model (mesh) remains smooth, and the roughness length scale represents the roughness, generally using k_s (equivalent sand grain roughness height) as a variable for a roughness function (ΔU^+) which will shift/modify the mean velocity profile. This method is only supported when using the RANSE (Reynolds-Averaged Navier–Stokes Equations). The modified wall function method is very effective for modeling large objects such as the hull of a ship, where the k_s and ΔU^+ values have been previously known and inputted, as was done by Demirel et al. [21], Song et al. [22], Andersson et al. [23], and also it can be used for propeller [24] and tidal turbine [25]. The modified wall function method prioritizes seeing results (impacts), such as increased drag, wake, and the like. Meanwhile, the geometrically resolved method used the real roughness geometry that formed from the mesh. These methods generally use to know how the k_s value and the ΔU^+ characteristic from a roughness. DNS (Direct Numerical Simulation) and LES (Large Eddy Simulation) are well known to be very good at doing this task. The geometrically resolved can also be done with RANSE as done by Atencio & Chernoray [26] with a difference of about 7% with their experimental results.

A reduction in hull performance due to roughness can be simulated using CFD with a modified wall function method with acceptable accuracy. Reynolds-averaged Navier–Stokes Equations (RANSE) simulation to study the friction resistance of flat plates due to the antifouling coating performed by Demirel et al. [27]. They used the roughness function from the experimental result of Schultz [28]. Using the Kriso Container Ship model, Demirel et al. [21] continued the CFD simulation to predict the impact of marine coatings and biofouling. Song et al. [22] also looked at the effect of biofouling on the ship's hydrodynamic characteristics, using a different roughness function. Anderson et al. [23] performed a comprehensive review and comparative analysis of different methods to model hull roughness. The comparison of acceptable CFD and experimental results was carried out by Song et al. [29].

Much of the literature reported assumes that the roughness distribution is homogeneous, but in reality, it is much non-homogeneous. Hull roughness, mainly that arising from biofouling, rarely occurs homogeneously. From a personal review in the field, the authors found that the biofouling growth was thicker in the stern of the vessel than in the bow, which may be influenced by the distribution of shear stress and flow compressive forces, which are more favorable for biofouling to grow better at the stern [30].

Many studies are looking at the roughness problems at an inhomogeneous pattern. The smooth-to-rough and rough-to-smooth patterns in streamwise direction were studied by Antonia & Luxton [31, 32]. In a streamwise phenomenon, the flow of fluid through abruptly different roughness conditions produces an internal boundary layer, which limits the near-wall layer, which senses the new surface conditions, from the flow further away from the wall, which keeps a memory of the upstream surface conditions before the surface transition [33]. The internal boundary layer and the local wall shear stress, at the transition of the two difference roughness conditions, exceed the equilibrium value when the roughness is homogeneous and then change to relax according to the homogeneous roughness equilibrium value certain distance [34]. Experimental methods and numerical simulations carried out several studies related to this inhomogeneous roughness. However, the numerical simulations for solving this case are mostly DNS and LES. Few do that through the RANSE, as Suastika et al. [35] on a flat plate, and Song et al. [36] using the Wigley hull model.

The frictional resistance acting on the hull due to inhomogeneous roughness becomes important to be modeled and analyzed, considering that the hull roughness

due to biofouling is mostly inhomogeneous. In a simple method where the ship hull is represented by a flat plate, then an inhomogeneous roughness is applied by dividing the plate into three equal parts, namely the fore, middle, and after. The parts are given different roughness values in the form of k_s and are arranged according to several combinations. From the simulation results on inhomogeneous roughness in the form of frictional resistance values will be compared with where if the condition is a smooth surface and some surfaces with homogeneous roughness. Then how are the three roughness values in the inhomogeneous condition correlated to become one roughness value (homogenized) which is close to the inhomogeneous roughness value. This CFD simulation uses the basis of Reynolds-averaged Navier–Stokes Equations (RANSE), where the roughness model uses a modified wall function. Research with variations in roughness that is streamwise inhomogeneous, which is then analyzed systematically, according to our knowledge is still a little done.

2. CFD modeling

A Reynolds-averaged Navier–Stokes Equations (RANSE) model, implemented in ANSYS Fluent, was used to solve the governing equations that can model turbulent flow over rough walls using modified wall function. The governing equations consist of averaged continuity and momentum equations, which for an incompressible flow without body forces, are given using tensor notation as described in Eqs. 5 and 6, respectively. Where i,j = 1, 2, 3, U_i is the mean velocity component, P is the mean pressure, ρ is the fluid density, ν is the kinematic viscosity, u_i' is the fluctuating velocity component, and $\overline{u_{i'}u_{j'}}$ is the Reynolds stresses [37].

$$\frac{\partial U_i}{\partial x_i} = 0 \tag{5}$$

$$\frac{\partial U_i}{\partial t} + \frac{\partial \left(U_i U_j\right)}{\partial x_j} = -\frac{1}{\rho}\frac{\partial P}{\partial x_i} + \frac{\partial}{\partial x_j}\left[\nu\left(\frac{\partial U_i}{\partial x_j} + \frac{\partial U_j}{\partial x_i}\right)\right] - \frac{\partial\left(\overline{u_{i'}u_{j'}}\right)}{\partial x_j} \tag{6}$$

The realizable k–ε with standard wall function turbulence model, which relates the Reynolds stresses to the mean flow properties, was used to close the system of Eqs. (5) and (6). The turbulence model is a two-equation model representing the transports of turbulence kinetic energy k and turbulence dissipation rate ε [38].

The roughness function (ΔU^+) model used in this study is that proposed by Cebeci and Bradshaw [39], whose model follows Nikuradse's uniform sand-grain roughness data [19]. Therefore, the roughness height utilized in this study is referred to as equivalent sand-grain roughness height k_s. The generalized Cebeci and Bradshaw's roughness function model is given in Eq. (7), where A = 0, $k^+_{s;smooth}$ = 2.25, $k^+_{s;rough}$ = 90.00 and C_s = 0.253. In which the power a is given in Eq. (8).

$$\Delta U^+ = \begin{cases} 0 & \rightarrow k_s^+ \le k^+_{s;smooth} \\ \frac{1}{\kappa}\ln\left[A\left(\frac{k_s^+/k^+_{s;smooth}}{k^+_{s;rough} - k^+_{s;smooth}}\right) + C_s k_s^+\right]^a & \rightarrow k^+_{s;smooth} < k_s^+ \le k^+_{s;rough} \\ \frac{1}{\kappa} ln\left(A + C_s k_s^+\right) & \rightarrow k_s^+ > k^+_{s;rough} \end{cases} \tag{7}$$

$$a = \sin\left[\frac{\pi}{2}\frac{\log\left(k_s^+/k_{s;smooth}^+\right)}{\log\left(k_{s;rough}^+/k_{s;smooth}^+\right)}\right] \tag{8}$$

The boundary conditions were set for this study, as illustrated in **Figure 1a**. The inlet was velocity inlet where the free stream velocity prescribes the flow velocity U_∞. The outlet was the pressure outlet set to be hydrostatic to ensure no upstream propagation of disturbances. The no-slip condition is applied on the plate's surface while the top and side boundaries are modeled as free-slip walls. The boundary conditions, governing, and turbulence modeling equations are discretized using a finite volume second-order method. These sets are then solved using a finite volume solver, utilizing a SIMPLE algorithm in which gradient calculations are carried out using the least-square cell-based method. The residual is set at 10^{-5} as a convergence criterion. For all simulations in this study, the plate length, fluid properties, and free stream velocity are kept constant. The plate length L is 30 m. The fluid is seawater with mass density ρ = 1025 kg/m^3 and dynamic viscosity μ = 0.001077 kg/(ms). Finally, the free stream velocity is set at U_∞ = 9.77 m/s (19 knots).

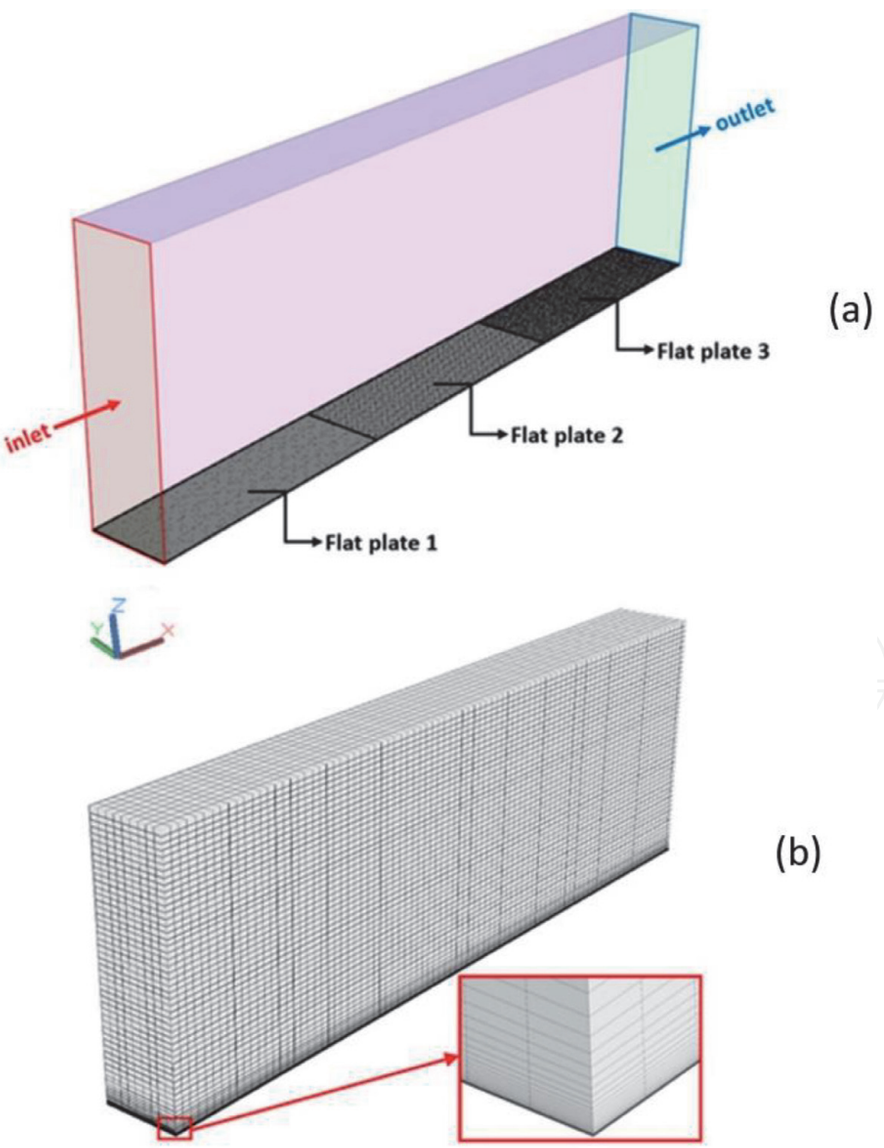

Figure 1.
The flow domain used in the simulations with three plate segments at the bottom boundary (a), and the hexahedron mesh with an exponential cell height gradation near the wall bottom boundary (b).

In CFD modeling, the distance of the frame against the wall is set to decrease exponentially as it moves typically towards the wall., as shown in **Figure 1b**. A hexahedron-type mesh is chosen, and it is arranged manually with adjustable grid size. It is crucial to determine the mesh size near the wall to obtain an appropriate value for the dimensionless normal coordinate y^+, defined as $y^+ = u\tau y/\nu$, where y is the outward wall-normal coordinate. To model the roughness effects correctly, the y^+ value for the first cell center above the wall must be larger than the local roughness Reynolds number k_s^+. To ensure this condition is always satisfied, ANSYS Fluent will virtually shift the wall if $y^+ < k_s^+$. For the roughness cases considered in this study, a blockage effect of 50% of the roughness height is assumed, and the corrected y^+ value for the first cell center above the wall is given as $y^+ = y^+ + k_s^+/2$. In this way, the singularity issue is avoided, and fine meshes can be handled correctly.

3. Surface roughness modeling

In this study, we will investigate just single parameter variations, namely the roughness height k_s. This section will explain details of the k_s set up and their possible combinations. Four surface roughness with different k_s values are considered in this study, namely, smooth wall (S), small roughness height (P), medium roughness height (Q), and high roughness height (R). All three combinations of roughness P, Q, and R are considered to form either homogeneous or inhomogeneous rough walled turbulent boundary layer flow. For example, a three-surface combination of PPP, QQQ, or RRR forms a homogeneous roughness, while a combination of PQR, PRQ, QPR, etc., forms an inhomogeneous roughness, where those are described in **Figure 2**. These k_s values are specifically chosen so that the average height of three different k_s of P = 81.25 μm, Q = 325.00 μm, and R = 568.75 μm will give an average height equal of Q, i.e., (81.25 μm + 325.00 μm + 568.75 μm)/3 = 325.00 μm. The selected k_s values are also designed to simulate the various stages of ship-hull biofouling growth, ranging from light slime [16] to about small calcareous fouling [15].

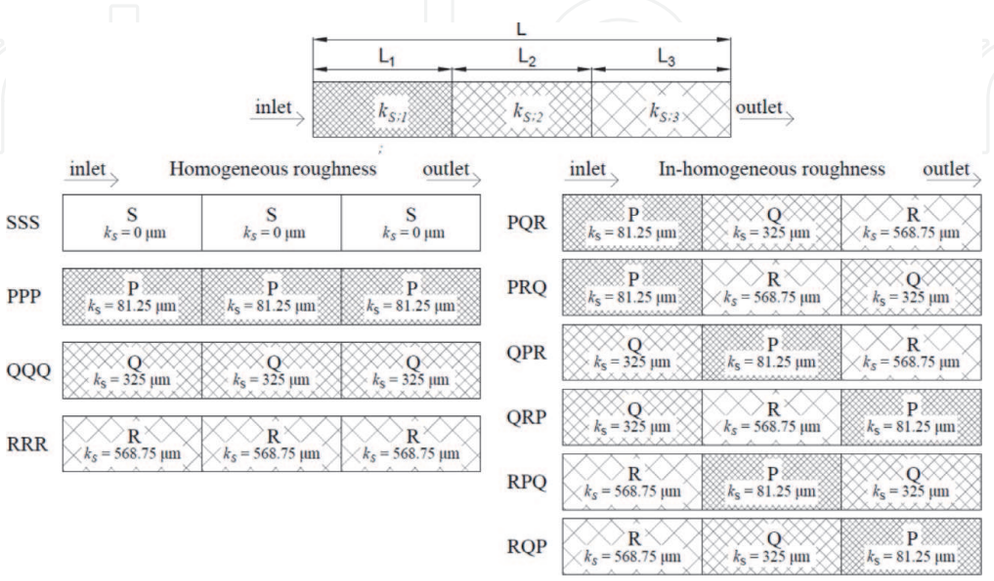

Figure 2.
Combinations of three plate segments resulting inhomogeneous (including fully smooth) and inhomogeneous rough surface conditions.

4. Verification and validation of modeling results

4.1 Grid independence study

To ensure optimum numbers of cells are used in the final simulations, several grid independence tests using flat plate smooth wall (SSS) base cases are conducted. For each case, the overall friction coefficient C_F is calculated using the increasing number of cells in the simulation. The number of cells in the latter simulation is approximately twice than that in the former. The overall friction coefficient C_F is defined in Eq. (9), where D is the drag per unit width, τ_w is the wall shear stress, ρ is the fluid density, U_∞ is the free stream velocity, L is the plate length, and x is the distance downstream from the leading edge of the plate. Furthermore, a percent error $e_{n+1,n}$ between the lower and higher cell numbers is defined in Eq. (10) [40].

$$C_F = \frac{D}{\rho U_\infty{}^2 L/2} = \frac{\int_0^L \tau_w dx}{\rho U_\infty{}^2 L/2} \tag{9}$$

$$e_{n+1,n} = \frac{C_F(n+1) - C_F(n)}{C_F(n)} \times 100\% \tag{10}$$

The results of the grid independence study are summarized in **Table 1**. The number of cells is varied from 750,000 to 6,127,550. **Table 1** shows that the C_F value increases monotonically with the increasing number of cells, which is expected to reach an asymptotic value at a very large number of cells. The value of $e_{n+1,n}$ as listed in **Table 1** decreases with the increasing number of cells used in the simulation. The results show that the error is very low (in the range 0.0206–0.131%), well below the recommended 2% from the literature [41]. Based on this grid independence test, N = 3,000,000 is chosen as an optimum number of cells for all the cases (including homogeneous and inhomogeneous roughness).

4.2 Verification and validation

In addition to the grid independence tests, further analyses are carried out for varied viscous-scaled wall-normal distance y^+ ranges of the first cell center above the wall. For the smooth plate SSS case, the calculation result is verified using the well-known Schoenherr's friction coefficient and the 1957 ITTC (International Towing Tank Conference) ship-model correlation line. Schoenherr's friction coefficient C_F is given in Eq. (11). It was adopted by ATTC (American Towing Tank Conference) as a standard for the clean hull skin friction resistance in 1947, and it is often referred to as the 1947 ATTC line. The second correlation is the 1957 ITTC ship-model correlation line, which is given in Eq. (12). A percent error is defined

Run number n	Number of cells N	$C_F \times 10^3$	Percent error $e_{n+1,n}$ [%]
1	500,000	1.788	—
2	1,522,950	1.790	0.1310
3	3,000,000	1.791	0.0332
4	6,127,550	1.791	0.0206

Table 1.
Friction coefficients C_F calculated using increasing number of cells in the simulations for the smooth plate (SSS).

Case	Re_L	$C_{F;1}$	$C_{F;2}$	$C_{F;3}$	C_F	$e_{r;s}$	$e_{i;q}$	$e_{i,h}$
		$\times 10^3$	$\times 10^3$	$\times 10^3$	$\times 10^3$	[%]	[%]	[%]
H30_SSS	2.79×10^8	2.075	1.700	1.596	1.790	0.00		
H30_PPP	2.79×10^8	2.608	2.062	1.915	2.195	22.60		
H30_QQQ	2.79×10^8	3.436	2.660	2.455	2.850	59.19	0.00	
H30_RRR	2.79×10^8	3.809	2.918	2.685	3.137	75.23		
I30_PQR	2.79×10^8	2.607	2.736	2.759	2.700	50.82	−5.26	1.87
I30_PRQ	2.79×10^8	2.607	3.037	2.473	2.706	51.12	−5.07	1.71
I30_QPR	2.79×10^8	3.437	2.007	2.770	2.738	52.92	−3.94	0.37
I30_QRP	2.79×10^8	3.436	2.951	1.846	2.745	53.29	−3.71	−0.44
I30_RPQ	2.79×10^8	3.811	1.988	2.484	2.761	54.21	−3.13	−0.52
I30_RQP	2.79×10^8	3.810	2.633	1.846	2.763	54.32	−3.06	−1.14

Table 2.
Overall friction coefficients for the plate segments $C_{F;1}$, $C_{F;2}$, $C_{F;3}$ and the entire plate C_F, and the percent errors $e_{r;s}$, $e_{i;q}$ and $e_{i,h}$.

Case	Re_L	y^+ range		$C_F \times 10^3$			Percent error [%]	
		Min	Max	CFD	ATTC'47	ITTC'57	ATTC'47	ITTC'57
SSS	2.79×10^8	64	112	1.773	1.802	1.805	−1.56	−1.76
SSS	2.79×10^8	155	254	1.791	1.802	1.805	−0.62	−0.62

Table 3.
Overall friction coefficient C_F calculated using different ranges of y^+ value for the first cell center above the wall compared with 1947 ATTC (Eq. (11)) and 1957 ITTC (Eq. (12)) lines for the smooth SSS case.

between the CFD result and the 1947 ATTC line and, in a similar manner, between the CFD result and the 1957 ITTC ship-model correlation line to quantify the accuracy of the CFD results. The percent error e in the latter case is calculated using Eq. (13).

$$\frac{0.242}{\sqrt{C_F}} = \log_{10}(\mathrm{Re}\, C_F) \tag{11}$$

$$C_F = \frac{0.075}{\left[\log_{10}(\mathrm{Re}) - 2\right]^2} \tag{12}$$

$$e = \frac{C_{F;CFD} - C_{F;ITTC\ 1957}}{C_{F;ITTC\ 1957}} \times 100\% \tag{13}$$

The results are summarized in **Table 3**, showing C_F values calculated using different y^+ ranges for the first cell center above the wall targeted in the simulations. **Table 3** shows that for the SSS case, using a y^+ range between 155 and 254 would result in the closest C_F value to the 1947 ATTC and 1957 ITTC lines with percent errors of e = 0.620% and e = 0.814%, respectively. A smaller y^+ range will result in larger differences, but the percentage differences do not exceed 1.76%, which is relatively small. Despite these anomalies, overall, the CFD and the 1947 ATTC or the 1957 ATTC line are small. Despite some discrepancies, for the smooth surface cases considered in this study, any y^+ range between 64 and 254 will result in an acceptable C_F value with a maximum magnitude of percent errors of 1.57%

when compared with the 1947 ATTC line and 1.76% when compared with the 1957 ITTC line. This result is following the recommended y^+ range in the literature for smooth flat plate CFD simulations between 50 and 300 [42].

To model the roughness effects correctly, the y^+ value for the first cell center above the wall denoted as $(\Delta y^+)_1$, must be larger than the local equivalent sand grain roughness Reynolds number k_s^+, i.e., $(\Delta y^+)_1 > k_s^+$. However, when one employs a fine mesh near the wall, the $(\Delta y^+)_1$value may have a smaller value than the k_s^+value, i.e., $(\Delta y^+)_1 < k_s^+$. If such a case happens, ANSYS Fluent applies a virtual shift of the wall by increasing the value of $(\Delta y^+)_1$ with an amount $k_s^+/2$, such that $(\Delta y^+)_1 > k_s^+$.

To gain more insight into the CFD results for rough conditions, they are verified using the empirical calculation, Granville's similarity law scaling method [43]. The simplified Granville similarity scaling can be calculated using Eqs. 14, 15, and 16. Where: C_{F_R} is the coefficient of frictional resistance for rough condition, where the empirical formula as the foundation is taken from the approximated Kármán-Schoenherr formula [44]; Re_r is the Reynolds number for calculate the C_{F_R} using the empirical formula, which equal of the Reynolds number for smooth condition (Re_s) that is shifted as described in Eq. (15). Then, κ is the von Kármán constant; $k_s{}^+$ is roughness Reynolds number; ν is kinematic viscosity; U_τ is friction velocity defined as $\sqrt{\tau_w/\rho}$ or approached by $U_\infty(C_F/2)^{1/2}$; τ_w is the shear stress magnitude, where to get it is necessary to do iterative calculations against C_{F_R}. The roughness function ΔU^+ is from Cebeci and Bradshaw [39] in Eq. (7), according to this study.

The verification result using the similarity scaling from Granville [43] can be seen in **Table 4**. The calculation uses $e_{C;G}$, as described in Eq. (17). From the results of the calculation of $e_{C;G}$, it can be concluded that CFD modeling for homogeneous roughness can be accepted with the difference in error against the empirical is not exceed 1.8%.

$$C_{F_R} = \frac{0.0795}{\left(\mathrm{Log}_{10} Re_r - 1.729\right)^2} \tag{14}$$

$$Re_r = Re_s - 10^{\left(\frac{\Delta U^+ \kappa}{\ln(10)}\right)} \tag{15}$$

$$\Delta U^+ = f\left(k_s{}^+\right) = f\left(\frac{k_s U_\tau}{\nu}\right) \tag{16}$$

$$e_{C;G} = \frac{C_{F;CFD} - C_{F;Granville}}{C_{F;Granville}} \times 100\% \tag{17}$$

$$k_s^+ = \left(\frac{k_s}{L}\right)\left(\frac{Re\, C_{FS}}{2}\right)\left(\sqrt{\frac{2}{C_{FR}}}\right)\left[1 - \frac{1}{\kappa}\left(\sqrt{\frac{2}{C_{FR}}}\right) + \frac{1}{\kappa}\left(\frac{3}{2\kappa} - \Delta U^{+\prime}\right)\left(\frac{C_{FR}}{2}\right)\right] \tag{18}$$

Case	Re_L	$C_F \times 10^3$		$e_{C;G}$ [%]
		CFD	Granville	
PPP	2.79×10^8	2.195	2.191	0.20
QQQ	2.79×10^8	2.850	2.880	−1.03
RRR	2.79×10^8	3.138	3.195	−1.79

Table 4.
Overall friction coefficient C_F of homogeneous rough condition calculated compared with the similarity law scaling procedure from Granville [43].

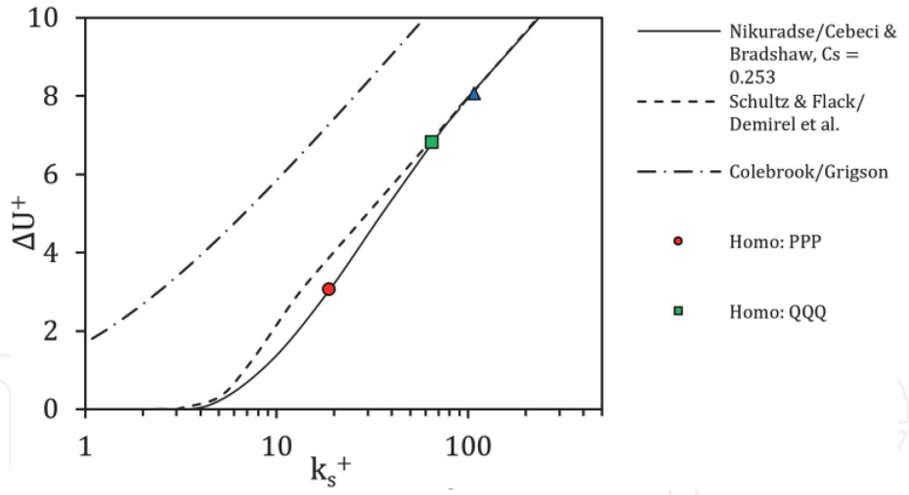

Figure 3.
ΔU^+ and k_s^+ for homogeneous cases that calculated using Granville [45] compared with the used roughness function, and other roughness functions, Colebrook-type roughness function [46], and Schultz and Flack [47].

$$\Delta U^+ = \left(\sqrt{\frac{2}{C_{FS}}}\right) - \left(\sqrt{\frac{2}{C_{FR}}}\right) - 19.7\left[\left(\sqrt{\frac{C_{FS}}{2}}\right) - \left(\sqrt{\frac{C_{FR}}{2}}\right)\right] - \frac{1}{\kappa}\,\Delta U^{+\prime}\left(\sqrt{\frac{C_{FR}}{2}}\right) \tag{19}$$

The homogeneous roughness simulation results were also verified using other literature from Granville [45], as written in Eqs. 18 and 19. This method can predict the characteristic roughness function, $\Delta U^+ = f\left(k_s{}^+\right)$, by plotting the predicted value of ΔU^+ (Eq. (19)) against $k_s{}^+$ (Eq. (18)) with the difference in the overall drag results from the rough conditions (C_{FR}) to the smooth conditions (C_{FS}). Where, L is the plate length, Re is the Reynolds number, k_s is the roughness height, and $\Delta U^{+\prime}$ is the roughness function slope, which is the slope of ΔU^+ as a function of $\ln\left(k_s{}^+\right)$. The verification results are plotted in **Figure 3** and the simulation results successfully approached the planned roughness function model, namely from Cebeci and Bradshaw [39], with C_s = 0.253. Verification of the simulation results using Granville [45] method described in **Figure 3**. The results collapse on the roughness function used (Cebeci and Bradshaw [39]).

5. Results and discussion

A systematic analysis of the results from the inhomogeneous rough surface cases is given in this section. To study the roughness effects, the local (c_f) and overall (C_F) skin friction coefficients are calculated for both the homogeneous and inhomogeneous roughness cases. The effects from the roughness height and the roughness sequence in the streamwise direction are studied by analyzing the plots of local skin friction coefficient as a function of the length and plotting the mean velocity profile for the step up and step-down phenomenon and by comparing its integral values (C_F) for the different cases. We also calculate the skin friction coefficient percentage differences between rough surfaces (both homogeneous and inhomogeneous) and the smooth wall reference case and between inhomogeneous roughness cases (combination of PQR) and the homogeneous roughness reference case (i.e., QQQ). Lastly, we carried out the prediction of how the single k_s value of the homogeneous case that equal to the three different k_s that composed the inhomogeneous case.

5.1 Local skin friction c_f

The local skin friction coefficient c_f is defined in Eq. (20). Where τ_w is the wall shear stress (obtained from CFD simulation), ρ is the fluid density and U_∞ is the free stream velocity. The streamwise length x and lateral position y for the inhomogeneous RPQ case are plotted in **Figure 4**. Generally, c_f is plotted against Re_x, but in this case, Re_x is represented by x (streamwise distance) because we want to study the step-up and step-down phenomena. The factors of streamwise length (L) and freestream velocity (U_∞), which are components of the Re_x value, have different effects on the increase in friction resistance [48].

$$c_f = \frac{\tau_w}{\rho U_\infty^2/2} \tag{20}$$

5.1.1 Homogeneous and inhomogeneous roughness

Figure 4 shows that the rough-wall homogeneous cases have a higher c_f than that of the smooth wall case at the same position on the streamwise. This value indicates that a rough wall surface indeed deviates from the smooth wall case and increases skin friction drag [19]. Within the homogeneous rough wall cases, the plots show that the highest k_s case (RRR) has a higher c_f value than those of the lower k_s cases (Q and P respectively) at equal place. Such behavior shows that a rougher surface will experience an elevated wall drag compared with less rough surfaces. The four homogeneous cases (including the smooth wall case) show a similar monotonic decrease in c_f with increasing x. This classical result of exponential decrease of c_f with x or Re_x illustrates large friction near the leading edge of the plate (low Reynolds numbers), which decreases exponentially towards the trailing edge. Similar behavior has been reported in various experimental and numerical studies [15, 49].

For the inhomogeneous cases with step changes in the equivalent sand grain roughness height k_s (PQR, PRQ, QPR, QRP, RPQ and RQP), the c_f values show step responses following the step-change in k_s. For example, **Figure 4a** with PQR step changes case show an increase in c_f every time there is an increase from P to Q and from Q to R height. **Figure 4a** shows that in the first one-third part of the inhomogeneous rough plate (0 m $< x <$ 10 m) with k_s value of 81.25 mm (P), the inhomogeneous case line (solid red line) collapses with the homogeneous PPP case (yellow dotted line) well. However, as the inhomogeneous case arrives at the start of the second one-third part of the plate (10 m $< x <$ 20 m), where it has k_s value of 325.00 μm (Q), the red line slightly jumps over (overshoots) the homogeneous QQQ case represented with a green dashed-dotted line, and then the red line gradually falls onto the homogeneous QQQ case. Finally, the last one-third part of the inhomogeneous rough plate (20 m $< x <$ 30 m) has k_s value of 568.75 μm (R), and the plot clearly shows that the red line slightly overshoots the homogeneous RRR case (dashed blue line) in the first few x and then gradually collapses to the homogeneous RRR case. Similar behavior is observed for all of the other five inhomogeneous roughness combinations (**Figure 4b–f**).

Such a jump in c_f, Andreopoulos and Wood [50] have reported values between one surface profile to another surface profile. They measured the response of a smooth wall boundary layer to a perturbation/disturbance caused by a short sandpaper strip. The measured τ_w behind the strip was around three times the undisturbed value (fully smooth case). The sudden jump in c_f is followed by a

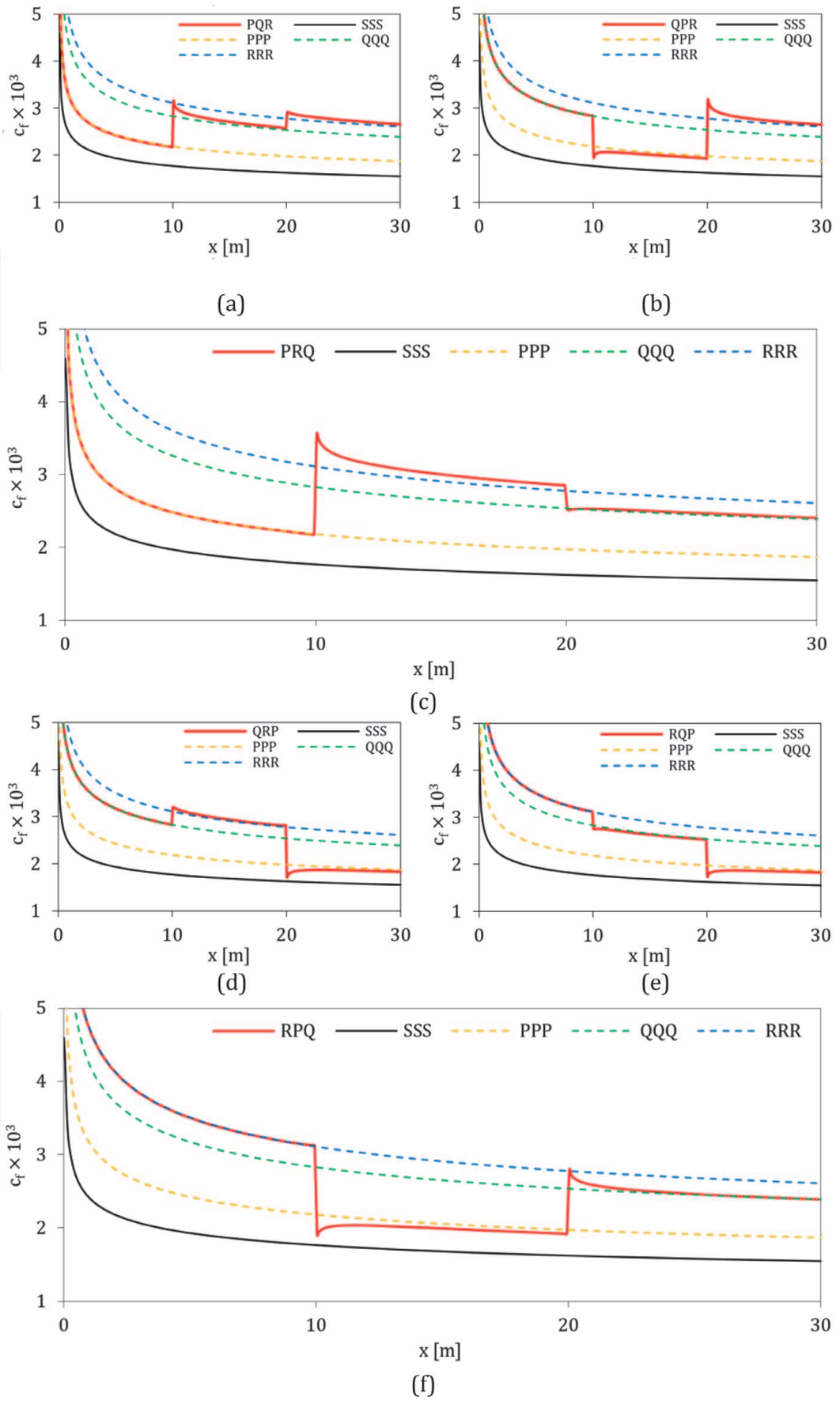

Figure 4.
The distribution of local skin friction coefficient c_f along the plate length for the inhomogeneous PQR (a), PRQ (c), QPR (b), QRP (d), RPQ (f), and RQP (e) cases compared with the homogeneous SSS, PPP, QQQ, and RRR cases.

relaxation, where the c_f is slowly returning to the smooth wall value. The relaxation rate was found to be very slow and Andreopoulos and Wood [50] were unable to record any full recovery, even at the last measuring point. As observed by Andreopoulos and Wood [50], our CFD results of local c_f shown in Figure 9 also exhibit a slow relaxation rate. However, RANSE cannot pick up the small-scale turbulence structures near the wall that occur at the border between the two roughness zones, influencing the flow downstream. The wall model cannot fully capture the flow physics, but it provides us with some indications of the effect. **Figure 4** indicate that the c_f value of the inhomogeneous rough surface will recover the underlying homogeneous rough wall c_f further downstream if the distance is sufficiently long. To quantify this, an averaged overshoot/undershoot will be defined and calculated in the following sub-subsection.

To see what happens to the overshoot and undershoot phenomena, the mean velocity profile of the difference c_f values are plotted in **Figure 5**. The mean velocity profile plot was taken at a distance of 10.25 m from the leading edge. The step-up case where the c_f value overshoot was taken in the PRQ (see **Figure 4c**) and RRR cases, while the step-down case, where the c_f value was undershot, was taken in the RPQ (see **Figure 4f**) and PPP cases. The outer scaling method is used to compare the mean velocity of the profile, where y is the vertical distance from the wall, δ is the thickness of the boundary layer taken 0.99 U_∞, U_∞ is the free stream velocity, and U is the velocity at each y. The plot results show that in the roughness step-up where overshoot occurs, the velocity profile is shifted upward (see **Figure 5a**). Conversely, in the roughness step-down, where there is an undershoot of the cf. value, the velocity profile is shifted downwards (see **Figure 5b**).

5.1.2 Overshoot and undershoot percentage differences

The overshoot and undershoot height of the flow seems to be based on the k_s of the following roughness. For example, when we look into the cases PQR and PRQ in the first row of **Figure 5a** and **5b**, the jump from P to Q is lower than that from P to R, resulting in a lower overshoot from P to Q than that from P to R. This also leads to a faster settling time for the P to Q jump than that for P to R case. Such behavior happens because R corresponds to a much higher k_s value than that corresponds to the Q case. Such undershoot and overshoot raise a question regarding how much is

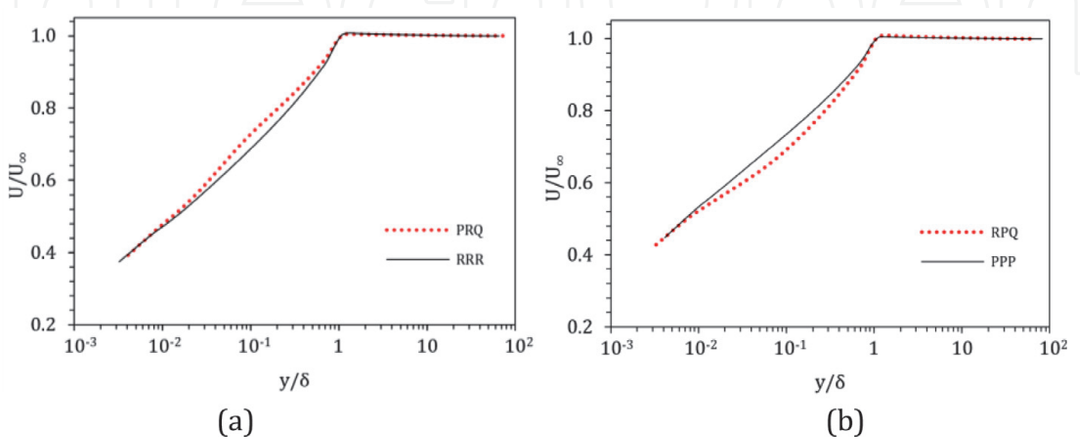

Figure 5.
Comparison of the mean velocity profile plot at x = 10.25 m from the leading edge with the outer scaling method to see the overshoot phenomenon for the step-up roughness (a), and undershoot for the step-down roughness (b).

the difference in c_f between the homogeneous and inhomogeneous cases. To answer such a question, a percent error $e_{i,h}$ is defined between the areas under the c_f curves for the inhomogeneous and homogeneous cases described in Eq. (21), where the subscripts h and i refer to homogeneous and inhomogeneous cases, respectively. The integral boundaries and the surface roughness for the homogeneous and inhomogeneous cases correspond to each other. For example, $e_{i,h}$ for the inhomogeneous case QPR is calculated as described in Eq. (22).

$$e_{i,h} = \frac{\int \left(c_{f;i} - c_{f;h}\right) \mathrm{d}\,\mathrm{Re}_x}{\int \left(c_{f;h}\right) \mathrm{d}\,\mathrm{Re}_x} \times 100\% \tag{21}$$

$$e_{i,h} = \frac{\int_0^{L_1} \left(c_{f;QPR} - c_{f;QQQ}\right) \mathrm{d}\,\mathrm{Re}_x + \int_{L_1}^{L_1+L_2} \left(c_{f;QPR} - c_{f;PPP}\right) \mathrm{d}\,\mathrm{Re}_x + \int_{L_1+L_2}^{L_2+L_3} \left(c_{f;QPR} - c_{f;RRR}\right) \mathrm{d}\,\mathrm{Re}_x}{\int_0^{L_1} c_{f;QQQ} \mathrm{d}\,\mathrm{Re}_x + \int_{L_1}^{L_1+L_2} c_{f;PPP} \mathrm{d}\,\mathrm{Re}_x + \int_{L_1+L_2}^{L_2+L_3} c_{f;RRR} \mathrm{d}\,\mathrm{Re}_x} \times 100\% \tag{22}$$

Eq. (21) shows that if the boundary layer responded to the step-change instantly and there is no overshoot/undershoot from the homogeneous roughness curve, $e_{i,h}$ would be zero. A positive value of $e_{i,h}$ means that on average, there is an overshoot while a negative value of $e_{i,h}$ means that there is an undershoot relative to the corresponding homogeneous curves. The values of $e_{i,h}$ are tabulated in **Table 2**.

Table 2 shows cases with decreasing magnitude of overshoot in the following order: PQR > PRQ > QPR and cases with decreasing magnitude of undershoot in the following order: RQP > RPQ > QRP. A consistent trend is observed in all the cases with different plate lengths. The most significant averaged overshoot (1.87%) and undershoot (1.14%) are observed (PQR and RQP, respectively).

5.2 Overall skin friction C_F

Following the local skin friction analysis from the previous subsection, it is desirable to estimate the overall skin friction coefficient C_F of the plates. This allows us to see the influence of individual roughness height k_s or the combination of it in a more global way. The overall skin friction coefficient C_F is given in Eq. (9). It is related to the local skin friction coefficient $c_f(x)$ by the relation described in Eq. (23).

$$C_F = \frac{\int_0^L c_f(x) \mathrm{d}x}{L} \tag{23}$$

The corresponding overall skin friction coefficients C_{F_s} for the plate segments 1, 2, and 3 are given, respectively, as described in Eq. (24). Where x is the distance in the streamwise direction with the origin at the leading edge of the plate. The lengths of plate segments 1, 2, and 3 are denoted as L_1, L_2 and L_3, respectively.

Table 2 summarizes the overall C_F and those for each plate segments ($C_{F;1}$, $C_{F;2}$, $C_{F;3}$). **Table 2** shows that for the homogeneous cases, both the smooth SSS and the three rough cases (PPP, QQQ, and RRR), the overall friction coefficient C_F decreases as the flow move from the upstream to downstream ($C_{F;1} > C_{F;2} > C_{F;3}$). The RRR case has the largest C_F among the three homogeneous roughness cases due to its highest k_s value.

5.2.1 Quantification of the overall skin friction between rough surface and smooth surface

Having obtained the overall skin friction C_F from individual plates, quantification the change in drag penalty between one case to another is made in a more

simplified way. The first analysis we are interested in quantifies the roughness wall effects (both homogenous and inhomogeneous cases) on the overall skin friction relative to the smooth wall case. A percent increase in overall skin friction $e_{r;s}$ due to roughness effects is defined as described in Eq. (24). The subscripts r and s refer to rough and smooth, respectively. The results are tabulated in **Table 2**.

$$e_{r;s} = \frac{C_{Fr} - C_{Fs}}{C_{Fs}} \times 100\% \tag{24}$$

Table 2 shows that the RRR case results in the highest $e_{r;s}$ due to the highest k_s with a value of 75.23%. For the same reasons, the smallest $e_{r;s}$ resulted from the H240_PPP case, with a value of 18.65%. It is interesting to note that the homogeneous H120_QQQ case with k_s = 325 μm experienced an increase in drag penalty of 52.62% compared to the smooth wall case. Such a value of roughness height represents heavy slime [16] or fouled with light calcareous tube-worm fouling [51].

A similar rough and smooth wall $e_{r;s}$ analysis is also conducted for the inhomogeneous cases. The results show that the homogenous QQQ case (with k_s = 325 μm has a higher percent increase in overall skin friction $e_{r;s}$ than the inhomogeneous cases. Although the averaged roughness heights for the inhomogeneous cases are the same as the QQQ roughness height, their representative roughness heights are smaller than the QQQ roughness height and depend on the sequence roughness heights in the streamwise direction. It is observed that the values of $e_{r;s}$ for the inhomogeneous cases increase monotonically in the following order: PQR < PRQ < QPR < QRP < RPQ < RQP.

5.2.2 Quantification of the overall skin friction between inhomogeneous and homogeneous rough surface

Apart from looking at the percent increase in overall skin friction $e_{r;s}$ between the rough wall and smooth wall, it is also desirable to quantify the effects of roughness inhomogeneity (combination of PQR) on the overall skin friction C_F with respect to the homogeneous QQQ baseline case. For that purpose, a percent decrease between an inhomogeneous roughness case and the homogeneous QQQ case is defined in Eq. (25).

$$e_{i;q} = \frac{C_{F;i} - C_{F;QQQ}}{C_{F;QQQ}} \times 100\% \tag{25}$$

The subscript i refers to inhomogeneous roughness (variation of PQR) while the subscript QQQ refers to the homogenous rough wall base case. As has been noted above, the friction coefficient $C_{F;QQQ}$ is chosen as a reference because the arithmetic average of k_s for the inhomogeneous cases is equal to that of the homogeneous QQQ case. Calculating skin friction from measured surface roughness would normally use a single roughness value which generally comes from the average of measurements over the hull. Thus, $e_{i;q}$ represents the error of assuming a single (average) roughness value for an in-homogeneously rough hull. A negative value of $e_{i;q}$ indicates that the C_F values of the inhomogeneous cases (combination of PQR) are lower than the homogeneous base case (QQQ). The opposite is valid for a positive value of $e_{i;q}$. **Table 2** shows that the $e_{i;q}$ values are negative for all the inhomogeneous cases, indicating that the C_F values of all the inhomogeneous cases (combination of PQR) are lower than the homogeneous base case (QQQ). For the same plate length, the magnitude of $e_{i;q}$ decreases orderly in the sequence of PQR to RQP, indicating that the order of roughness arrangement plays a key role.

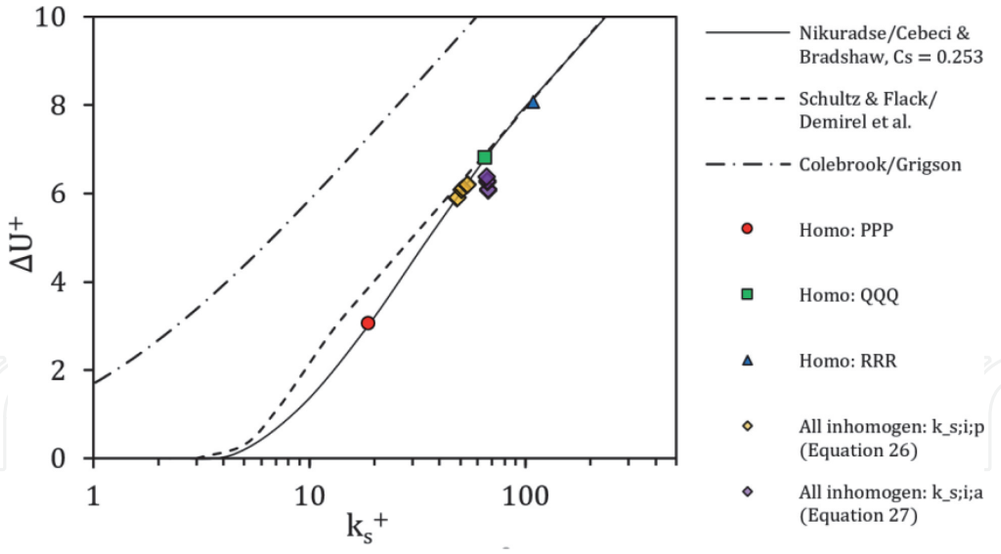

Figure 6.
Plotting the results of the verification of the predicted k_s values for inhomogenous cases with $k_{s;i;p}$ and $k_{s;i;a}$.

5.2.3 Prediction of a representative roughness height for an inhomogeneous rough surface

Having discussed the local and overall skin frictions, a question may arise: "Can we predict a representative roughness height k_s for an inhomogeneous rough surface?" We do this prediction with the help of the method from Granville [45], namely Eqs. 18 and 19, as well as the minimum error optimization help iterated by the solver to calculate the portion of each segment, L_1, L_2, and L_3. The result of this work creates Eq. (26), where it is found that the segment L_1 has a more significant portion, namely 29.7%. The L_2 segment has a portion of 24.3% and L3 $\approx$ 23.1%, where if all the portion of segments are totaled, the value will be smaller than the average value of the inhomogeneous k_s (see Eq. (27)), $k_{s;i;p} < k_{s;i;a}$.

$$k_{s;i;p} \approx 29.7\% \cdot k_{s;1} + 24.3\% \cdot k_{s;2} + 23.1\% \cdot k_{s;3} \tag{26}$$

$$k_{s;i;a} = \frac{k_{s;1} + k_{s;2} + k_{s;3}}{3} \tag{27}$$

The verification of the equation for predicting the k_s value for the inhomogeneous case is done with the aid of the Granville method [45], which plots the ΔU^+ and k_s^+, as explained in Eqs. (18 and 19), respectively. The results of the verification are plotted in **Figure 6**, where not only the results of the calculation $k_{s;i;p}$, but also the results of the calculation of $k_{s;i;a}$ are plotted. From the plot results, it can be seen that, prediction using $k_{s;i;p}$ got a very good match to the roughness function used in this simulation, namely from Cebeci and Bradshaw [39].

6. Conclusions

Rough-wall turbulent boundary layer flow is a complex physical phenomenon that increases skin friction drag compared to the smooth wall case. Because the surface roughness of a ship hull fouled with biofoulings or other types of hull imperfections is often found to be inhomogeneous, it is crucial to consider inhomogeneous roughness in addition to homogeneous roughness. In this study, the effects of roughness inhomogeneity on the skin friction drag are investigated by modeling

the inhomogeneous roughness pattern in a simplified manner using step changes in the equivalent sand grain roughness heights k_s, denoted as P, Q, and R.

Some of the findings from this study include:

- Such a step-change in the roughness height results in overshoot/undershoot of the local skin friction coefficient c_f, followed by a relaxation where the c_f value is slowly returning to the underlying rough wall homogeneous c_f value. A step up in k_s results in an overshoot, while a step down in k_s results in an undershoot in the c_f values. In some cases where the jump happens over two significantly different k_s values (i.e., P to R), the relaxation rate is very slow and unable to recover over the given streamwise distance fully. Cases with decreasing magnitude of overshoot are found in the following order: PQR > PRQ > QPR, and cases with decreasing magnitude of undershooting are in the following order: RQP > RPQ > QRP.

- The sequence of roughness arrangement in a streamwise inhomogeneous roughness pattern plays a key role in the resulting overall skin friction coefficient C_F. It is found that C_F increases in the following order: PQR < PRQ < QPR < QRP < RPQ < RQP. This result is further reflected in the predicted k_s values, showing k_s increases in the same order: PQR < PRQ < QPR < QRP < RPQ < RQP. A change of roughness near the leading edge of the plate has a much more significant effect on the overall skin friction coefficient C_F than a change of this near the trailing edge. In practical terms, limiting (cleaning) the biofouling from the bow of a ship is of greatest benefit and should be prioritized.

- The overall skin friction (C_F) in inhomogeneous cases (e.g. PQR) is smaller than the k_s value with the same mean. Thus, the mean value of k_s for the inhomogeneous case is less suitable for predicting the C_F value. A new way to predict the k_s value for the inhomogeneous case has been proposed in this paper (See Eq. (26)), where the value is very close to the simulation results that have been carried out.

Acknowledgments

This research project was supported by the Ministry of Research, Technology, and National Innovation and Research Agency (Kemenristek – BRIN) of the Republic of Indonesia under the World Class Professor 2019 Grant (Contract No. T/42/D2.3/KK.04.05/2019) and Master to Doctorate Program for Excellent Graduate (PMDSU) scholarship program batch III (Contract No. 1277/PKS/ITS/2020).

Conflict of interest

The authors declare that they have no known competing financial interests or personal relationships that could have appeared to influence the work reported in this paper.

Author details

I. Ketut Aria Pria Utama*, I. Ketut Suastika and Muhammad Luqman Hakim
Department of Naval Architecture, Institut Teknologi Sepuluh Nopember, Surabaya, Indonesia

*Address all correspondence to: kutama@na.its.ac.id

IntechOpen

References

[1] Hasan MI, Khafeef MJ, Mohammadi O, Bhattacharyya S, Issakhov A. Investigation of Counterflow Microchannel Heat Exchanger with Hybrid Nanoparticles and PCM Suspension as a Coolant. Menni Y, editor. Mathematical Problems in Engineering. 2021 Mar 23; 2021:1–12.

[2] Soni MK, Tamar N, Bhattacharyya S. Numerical simulation and parametric analysis of latent heat thermal energy storage system. Journal of Thermal Analysis and Calorimetry. 2020 Sep 4; 141(6):2511–26.

[3] Bhattacharyya S, Chattopadhyay H, Biswas R, Ewim DRE, Huan Z. Influence of Inlet Turbulence Intensity on Transport Phenomenon of Modified Diamond Cylinder: A Numerical Study. Arabian Journal for Science and Engineering. 2020 Feb 5;45(2):1051–8.

[4] Kumar S, Kumar R, Goel V, Bhattacharyya S, Issakhov A. Exergetic performance estimation for roughened triangular duct used in solar air heaters. Journal of Thermal Analysis and Calorimetry . 2021 May 24;

[5] Murmu SC, Bhattacharyya S, Chattopadhyay H, Biswas R. Analysis of heat transfer around bluff bodies with variable inlet turbulent intensity: A numerical simulation. International Communications in Heat and Mass Transfer . 2020 Oct;117:104779.

[6] Alam MW, Bhattacharyya S, Souayeh B, Dey K, Hammami F, Rahimi-Gorji M, et al. CPU heat sink cooling by triangular shape micro-pin-fin: Numerical study. International Communications in Heat and Mass Transfer . 2020 Mar;112:104455.

[7] Paul AR, Bhattacharyya S. Analysis and Design for Hydraulic Pipeline Carrying Capsule Train. Journal of Pipeline Systems Engineering and Practice . 2021 May;12(2):04021003.

[8] Suastika K, Hidayat A, Riyadi S. Effects of the Application of a Stern Foil on Ship Resistance: A Case Study of an Orela Crew Boat. International Journal of Technology . 2017 Dec 26;8(7):1266.

[9] Smith TWP, Jalkanen JP, Anderson BA, Corbett JJ, Faber J, et al. Third IMO Greenhouse Gas Study 2014. International Maritime Organization (IMO). 2014;

[10] Buhaug Ø, Corbett J., Endresen Ø, Eyring V, Faber J, Hanayama S, et al. Second IMO GHG Study2009. International Maritime Organization (IMO). 2009;

[11] Molland AF, Turnock SR, Hudson DA, Utama IKAP. Reducing ship emissions: A review of potential practical improvements in the propulsive efficiency of future ships. Transactions of the Royal Institution of Naval Architects Part A: International Journal of Maritime Engineering. 2014; 156(PART A2):175–88.

[12] Wang H, Lutsey N. Long-term potential to reduce emissions from international shipping by adoption of best energy-efficiency practices. Transportation Research Record. 2014; 2426:1–10.

[13] Kodama Y, Kakugawa A, Takahashi T, Kawashima H. Experimental study on microbubbles and their applicability to ships for skin friction reduction. International Journal of Heat and Fluid Flow. 2000;21 (5):582–8.

[14] Hakim ML, Nugroho B, Chin RC, Putranto T, Suastika IK, Utama IKAP. Drag penalty causing from the roughness of recently cleaned and

painted ship hull using RANS CFD. CFD Letters. 2020;12(3):78–88.

[15] Monty JP, Dogan E, Hanson R, Scardino AJ, Ganapathisubramani B, Hutchins N. An assessment of the ship drag penalty arising from light calcareous tubeworm fouling. Biofouling. 2016;32(4):451–64.

[16] Schultz MP. Effects of coating roughness and biofouling on ship resistance and powering. Biofouling. 2007;23(5):331–41.

[17] Hakim ML, Nugroho B, Nurrohman MN, Suastika IK, Utama IKAP. Investigation of fuel consumption on an operating ship due to biofouling growth and quality of anti-fouling coating. IOP Conference Series: Earth and Environmental Science. 2019; 339(1):012037.

[18] Schultz MP, Bendick JA, Holm ER, Hertel WM. Economic impact of biofouling on a naval surface ship. Biofouling. 2011;27(1):87–98.

[19] Nikuradse J. Laws of flow in rough pipes [English translation of Stromungsgesetze in rauhen Rohren]. VDI-Forschungsheft 361 Beilage zu "Forschung auf dem Gebiete des Ingenieurwesens" [Translation from NACA Technical Memorandum 1292]. 1933;

[20] Hama F. Boundary-layer characteristics for smooth and rough surfaces. Transactions - The Society of Naval Architects and Marine Engineers. 1954;62:333–58.

[21] Demirel YK, Turan O, Incecik A. Predicting the effect of biofouling on ship resistance using CFD. Applied Ocean Research. 2017;62:100–18.

[22] Song S, Demirel YK, Atlar M. An investigation into the effect of biofouling on the ship hydrodynamic characteristics using CFD. Ocean Engineering . 2019;175:122–37.

[23] Andersson J, Oliveira DR, Yeginbayeva I, Leer-Andersen M, Bensow RE. Review and comparison of methods to model ship hull roughness. Applied Ocean Research. 2020;99: 102119.

[24] Song S, Demirel YK, Atlar M. Penalty of hull and propeller fouling on ship self-propulsion performance. Applied Ocean Research. 2020;94: 102006.

[25] Song S, Shi W, Demirel YK, Atlar M. The effect of biofouling on the tidal turbine performance. Applied Energy Symposium: MIT A+B. 2019.

[26] Atencio BN, Chernoray V. A resolved RANS CFD approach for drag characterization of antifouling paints. Ocean Engineering. 2019;171:519–32.

[27] Demirel YK, Khorasanchi M, Turan O, Incecik A, Schultz MP. A CFD model for the frictional resistance prediction of antifouling coatings. Ocean Engineering. 2014;89:21–31.

[28] Schultz MP. Frictional Resistance of Antifouling Coating Systems. Journal of Fluids Engineering. 2004;126(6):1039–47.

[29] Song S, Demirel YK, Atlar M, Dai S, Day S, Turan O. Validation of the CFD approach for modelling roughness effect on ship resistance. Ocean Engineering. 2020;200:107029.

[30] Alamsyah MA, Hakim ML, Utama IKAP. Study of Shear and Pressure Flow on the Variation of Ship Hull Shapes as One of the Biofouling Growth Factors. In: Proceedings of the 3rd International Conference on Marine Technology. SCITEPRESS - Science and Technology Publications; 2018. p. 97–105.

[31] Antonia RA, Luxton RE. The response of a turbulent boundary layer to a step change in surface roughness

Part 1. Smooth to rough. Journal of Fluid Mechanics. 1971;48(4):721–61.

[32] Antonia RA, Luxton RE. The response of a turbulent boundary layer to a step change in surface roughness. Part 2. Rough-to-smooth. Journal of Fluid Mechanics. 1972;53(4):737–57.

[33] Chung D, Hutchins N, Schultz MP, Flack KA. Predicting the Drag of Rough Surfaces. Vol. 53, Annual Review of Fluid Mechanics. 2021.

[34] Pendergrass W, Arya SPS. Dispersion in neutral boundary layer over a step change in surface roughness —I. Mean flow and turbulence structure. Atmospheric Environment (1967). 1984;18(7):1267–79.

[35] Suastika IK, Hakim ML, Nugroho B, Nasirudin A, Utama IKAP, Monty JP, et al. Characteristics of drag due to streamwise inhomogeneous roughness. Ocean Engineering. 2021;223: 108632.

[36] Song S, Demirel YK, Muscat-Fenech CDM, Sant T, Villa D, Tezdogan T, et al. Investigating the effect of heterogeneous hull roughness on ship resistance using cfd. Journal of Marine Science and Engineering. 2021;9(2).

[37] Ferziger JH, Perić M. Computational Methods for Fluid Dynamics. Computational Methods for Fluid Dynamics. 2002.

[38] Shih T-H, Liou WW, Shabbir A, Yang Z, Zhu J. A new k-ϵ eddy viscosity model for high reynolds number turbulent flows. Computers & Fluids. 1995;24(3):227–38.

[39] Cebeci T, Bradshaw P. Momentum transfer in boundary layers. New York: Hemisphere Publishing Corporation; 1977.

[40] Mitchell R, Webb M, Roetzel J, Lu F, Dutton J. A study of the Base Pressure Distribution of a Slender Body of Square Cross-Section. In: 46th AIAA Aerospace Sciences Meeting and Exhibit. Reston, Virigina: American Institute of Aeronautics and Astronautics; 2008.

[41] Anderson J. Computational Fluid Dynamics: The Basics with Applications. 1995. McGrawhill Inc. 1995;

[42] Cant S. S. B. Pope, Turbulent Flows, Cambridge University Press, Cambridge, U.K., 2000, 771 pp. Combustion and Flame. 2001;125(4).

[43] Granville P. The Frictional Resistance and Turbulent Boundary Layer of Rough Surfaces. Journal of Ship Research. 1958;2(04):52–74.

[44] Schoenherr KE. Resistance of flat surfaces. Trans SNAME. 1932;40:40: 279-313.

[45] Granville PS. Three Indirect Methods for the Drag Characterization of Arbitrarily Rough Surfaces on Flat Plates. Journal of Ship Research. 1987;31 (1):70–7.

[46] Flack KA, Schultz MP, Rose WB. The onset of roughness effects in the transitionally rough regime. International Journal of Heat and Fluid Flow. 2012;35:160–7.

[47] Schultz MP, Flack KA. The rough-wall turbulent boundary layer from the hydraulically smooth to the fully rough regime. Journal of Fluid Mechanics. 2007;580:381–405.

[48] Moody LF. Friction factors for pipe flow. Transaction of the ASME. 1944;66: 671–84.

[49] Demirel YK, Uzun D, Zhang Y, Fang HC, Day AH, Turan O. Effect of barnacle fouling on ship resistance and powering. Biofouling. 2017;33(10):819–34.

[50] Andreopoulos J, Wood DH. The response of a turbulent boundary layer

to a short length of surface roughness. Journal of Fluid Mechanics. 1982;118 (1):143.

[51] Monty JP, Dogan E, Hanson R, Scardino AJ, Ganapathisubramani B, Hutchins N. An assessment of the ship drag penalty arising from light calcareous tubeworm fouling. Biofouling. 2016;32(4):451–64.